



Experimental study of the air–water shear flow in a hydraulic jump

H. Chanson*, T. Brattberg

Department of Civil Engineering, The University of Queensland, Brisbane QLD 4072, Australia

Received 17 July 1998; received in revised form 15 March 1999

Abstract

Although the hydraulic jump has been investigated experimentally for nearly two centuries, little information is known of the air–water flow properties in the shear region. New experiments were performed in a horizontal channel with partially-developed inflow conditions. Distributions of air concentration, mean air–water velocity and bubble frequency were recorded and presented herein. The results indicate an advective diffusion of air in the shear layer. The velocity profiles have a similar shape as wall jet flows but different quantitative parameters must be introduced. The relationship between air content and bubble frequency has a parabolic shape which is not yet understood but was observed previously in open channel flows. © 2000 Elsevier Science Ltd. All rights reserved.

Keywords: Air bubble entrainment; Hydraulic jump; Void fraction; Air–water velocity; Bubble frequency; Air–water shear flow; Experimental data

1. Introduction

In open channels, the transition between supercritical and subcritical flow (i.e. a hydraulic jump) is characterised by a sharp rise in free-surface elevation, strong turbulence, splashing and air entrapment in the roller. Historically air entrainment in hydraulic jump was investigated in terms of the air demand: i.e., the total quantity of entrained air (e.g. Wood, 1991; Chanson, 1997a). A ‘milestone’ contribution was the work of Resch and Leutheusser (1972) who showed first that the air entrainment process, the transfer of momentum and the energy dissipation are strongly affected by the inflow conditions. Recently, the first author (Chanson and Qiao, 1994;

* Corresponding author. Tel.: +61-7-3365-3516; fax: +61-7-3365-4599.

E-mail address: h.chanson@mailbox.uq.edu.au (H. Chanson).

Table 1
Experimental investigations of hydraulic jump flows

Reference	Flow conditions ^a	Measurement (measurement technique)	Comments
Rajaratnam (1965)	$2.68 \leq Fr_1 \leq 9.78$ $1.954 \leq V_1 \leq 3.99$ m/s $0.01548 \leq d_1 \leq 0.0613$ m P/D inflow conditions	Velocity (Prandtl-Pitot tube)	$W = 0.308$ m Pitot tube: 3-mm external diameter
Resch and Leutheusser (1972)	$Fr_1 = 2.98$ and 8.04 $V_1 = 1.84$ and 2.78 m/s $d_1 = 0.039$ and 0.012 m $x_1 = 0.39$ and 0.112 m P/D inflow conditions	Air content, velocity, velocity fluctuations (hot-film)	$W = 0.39$ m Conical hot-film probe DISA 55A87 (0.6-mm sensor size)
Thandaveswara (1974)	$Fr_1 = 3.26$ and 7.32 $V_1 = 2.5$ and 2.0 m/s $d_1 = 0.039$ and 0.012 m $x_1 = 2.44$ and 7.8 m F/D inflow conditions	Air content (conductivity probe), velocity (Pitot tube and conductivity probe)	$W = 0.6096$ m Pitot tube: 3.2-mm external diameter Conductivity probe: double tip
Reif (1978)	$Fr_1 = 7.16$ to 13.31 $V_1 = 2.18$ to 4.60 m/s $d_1 = 0.0107$ to 0.152 m $x_1 = 0.23$ m P/D inflow conditions	Velocity, velocity fluctuations (LDV) ^b	$W = 0.1$ m LDV DISA-55L (15 mW He–Ne laser tube) Polymer additive: polyacrylamide Calgon TRO-375 (0 and 100 ppm)
Babb and Aus (1981)	$Fr_1 = 2.0$ $x_1 = 0.1$ m P/D inflow conditions	Velocity, velocity fluctuations (LDV) ^b	$W = 0.1$ m LDV DISA-55L (15 mW He–Ne laser tube) Polymer additive: polyacrylamide Calgon TRO-375 (0 and 100 ppm)
Babb and Aus (1981)	$Fr_1 = 6.0$ $V_1 = 3.51$ m/s $d_1 = 0.035$ m	Air content, velocity, velocity fluctuations (hot-film)	$W = 0.46$ m Conical hot-film probe DISA 55R42 (0.4-mm sensor size)
Ohtsu et al. (1990)	$2.5 \leq Fr_1 \leq 9.5$ P/D inflow conditions	Velocity (Prandtl-Pitot tube?)	Case (a). $W = 0.15$ m

Imai and Nakagawa (1992) ^c	$Fr_1 = 3.7$ and 6.5 $V_1 = 1.94$ and 2.76 m/s $d_1 = 0.0281$ and 0.0184 m $x_1 = 1.4$ and 0.65 m	Velocity (Pitot tube and propeller)	$W = 0.3$ m Pitot tube: 3-mm external diameter Propeller: 3-mm external diameter
Hager (1992) Chanson and Qiao (1994) and Chanson (1995a,b)	$4.3 \leq Fr_1 \leq 8.9$ $Fr_1 = 5.0$ to 8.1 $V_1 = 1.975$ to 3.19 m/s $d_1 = 0.016$ to 0.017 m $x_1 = 0.7$ to 0.96 m P/D inflow conditions	Velocity (Propeller?) Velocity (Pitot tube), void fraction (conductivity probe)	$W = 0.5$ m $W = 0.25$ m Pitot tube: 3.3-mm external diameter Conductivity probe: single tip (0.35-mm inner electrode)
Wu and Rajaratnam (1996)	$Fr_1 = 3.87$ and 10.48 $V_1 = 1.56$ and 4.22 m/s $d_1 = 0.0165$ m P/D inflow conditions	Velocity (Prandtl-Pitot tube)	$W = 0.466$ m Pitot tube: 3-mm external diameter
Mossa and Tolve (1998)	$Fr_1 = 6.42, 6.45$ and 7.33 $V_1 = 2.85, 2.87$ and 3.12 m/s $d_1 = 0.02, 0.02$ and 0.0185 m P/D inflow conditions	Void fraction (video-camera image processing)	$W = 0.40$ m
Present study	$Fr_1 = 6.33$ and 8.48 $V_1 = 2.34$ and 3.14 m/s $U_1 = 2.58$ and 3.47 m/s $d_1 = 0.014$ m $x_1 = 0.5$ m P/D inflow conditions	Void fraction, air–water velocity, bubble frequency (conductivity probe)	$W = 0.25$ m Conductivity probe: double tip (25- μ m inner electrode).

^a P/D: partially developed inflow conditions; F/D: fully-developed inflow conditions.

^b LDV: laser Doppler velocimeter.

^c Also Nakagawa (1996).

Chanson, 1995a,b) studied particularly the air–water properties in partially-developed hydraulic jumps and he showed a similarity with plunging jet entrainment.

Past investigations were usually performed with Prandtl-Pitot tubes, propeller, LDV anemometer and hot-film probes (Table 1). Most of the measurement devices could be significantly affected by the air bubble entrainment and some hot-film probe data were very crudely processed (e.g. Resch and Leutheusser, 1972). Few studies provided accurate air–water flow measurements (e.g. Chanson, 1995a; Mossa and Tolve, 1998). Up to date, the air bubble diffusion process and the mechanisms of momentum transfer in the air–water flow of hydraulic jumps are not yet fully understood.

It is the purpose of this work to present new experimental results, to compare these with existing data (Table 1), and to present new compelling conclusions regarding momentum and void fraction development of jump-entrained air–water flows. The study is focused in the developing air–water flow region (i.e. $(x - x_1)/d_1 < 50$) of hydraulic jumps with partially-developed inflow conditions.

2. Experimental apparatus

The experiments were performed in a 3.2-m long horizontal channel of uniform rectangular section (Chanson and Qiao, 1994; Chanson, 1995a), Fig. 1. The flume is 0.25-m wide, the sidewalls are 0.30-m high and both walls and bed are made of glass. Regulated flows are supplied through an adjustable vertical sluice gate. During the experiments, the gate opening was fixed at 20 mm. The experimentally observed values for the coefficient of contraction were about 0.6. Tailwater levels were controlled by an overshoot sharp-crested gate at the downstream end of the channel.

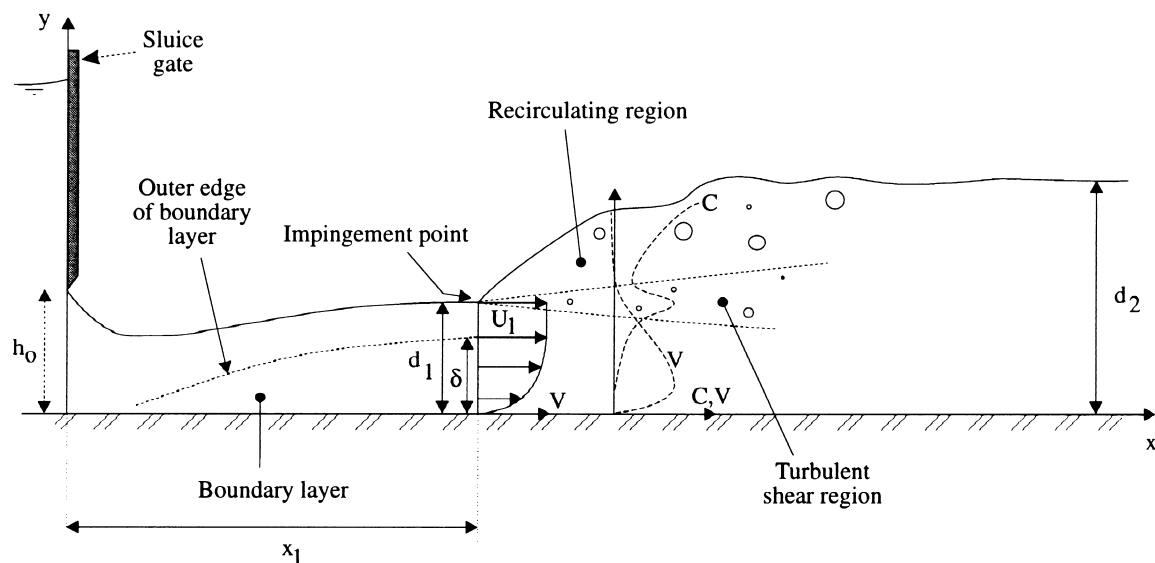


Fig. 1. Sketch of the hydraulic jump flow experiment.

The water was supplied by a constant head tank. The discharge was measured by a 90-degree V-notch weir, previously calibrated. The percentage of error is expected to be less than 2%.

The air–water flow properties were recorded using a dual-tip conductivity probe, the two tips being aligned in the flow direction. Each tip has an internal concentric electrode ($\varnothing = 25 \mu\text{m}$, Platinum electrode) and an external stainless steel electrode of $200 \mu\text{m}$ diameter. The probe was excited by an air bubble detector (Ref. AS25240) and the signals were scanned at 20 kHz per channel for 10 s. The analysis of the data provided the void fraction, mean air–water interface velocity and air bubble frequency.

In addition, clear water jet velocities and turbulent velocity fluctuations (in clear-water) were measured with a Pitot tube (external diameter $\varnothing = 3.3 \text{ mm}$) connected to a pressure transducer (Validyne[™] DP15). The transducer was scanned at 500 Hz and the accuracy of the clear-water velocity data was normally estimated as: $\Delta V/V = 1\%$. The translation of the probes in the direction perpendicular to the channel bottom was controlled by a fine adjustment travelling mechanism connected to a Mitutoyo[™] digimatic scale unit (Ref. No. 572-503). The error on the vertical position of the probes (i.e. Pitot tube and conductivity probes) was less than 0.01 mm. The longitudinal and transversal translations of the probes were controlled manually: the probes and the digimatic scale unit were fixed to a stiff L-shape aluminium beam fixed on a trolley system. The error on the longitudinal location of the probes was less than 5 mm. The error on the transverse location of the probes was less than 0.5 mm. Note that most measurements were taken on the channel centreline.

2.1. Discussion

Previous studies (Chanson and Qiao, 1994; Chanson, 1995a) were conducted with a single-tip conductivity probe ($\varnothing = 0.35 \text{ mm}$) and analog sampling times ranging from 60 to 300 s. During the present study, the data were digitally sampled at 20,000 Hz per channel for 10 s. Initial tests were conducted for the same flow conditions as Chanson and Qiao (1994) and Chanson (1995a), and they showed no difference in air concentration distributions. Higher bubble frequencies were observed consistently because the probe had a smaller sensor size (i.e. $\varnothing = 25 \mu\text{m}$).

Two series of experiments were performed (Table 1). In each case, the jump toe was located at $x_1 = 0.5\text{-m}$ downstream of the gate (Fig. 1) and the inflow was partially-developed: i.e., $\delta/d_1 \approx 0.65$ for both experiments, where δ is the boundary layer thickness and d_1 is the upstream flow depth. The result was obtained with Pitot tube measurements and it is consistent with previous results (Chanson and Qiao, 1994, Fig. 4-2).

Full details of the experimental results are reported in Chanson and Brattberg (1997).

3. Experimental results: void fraction distribution

3.1. Air–water flow regions

The air–water flow of the hydraulic jump is characterised by a turbulent shear region and a recirculating flow region above (Fig. 1). In the turbulent shear region, momentum is exchanged

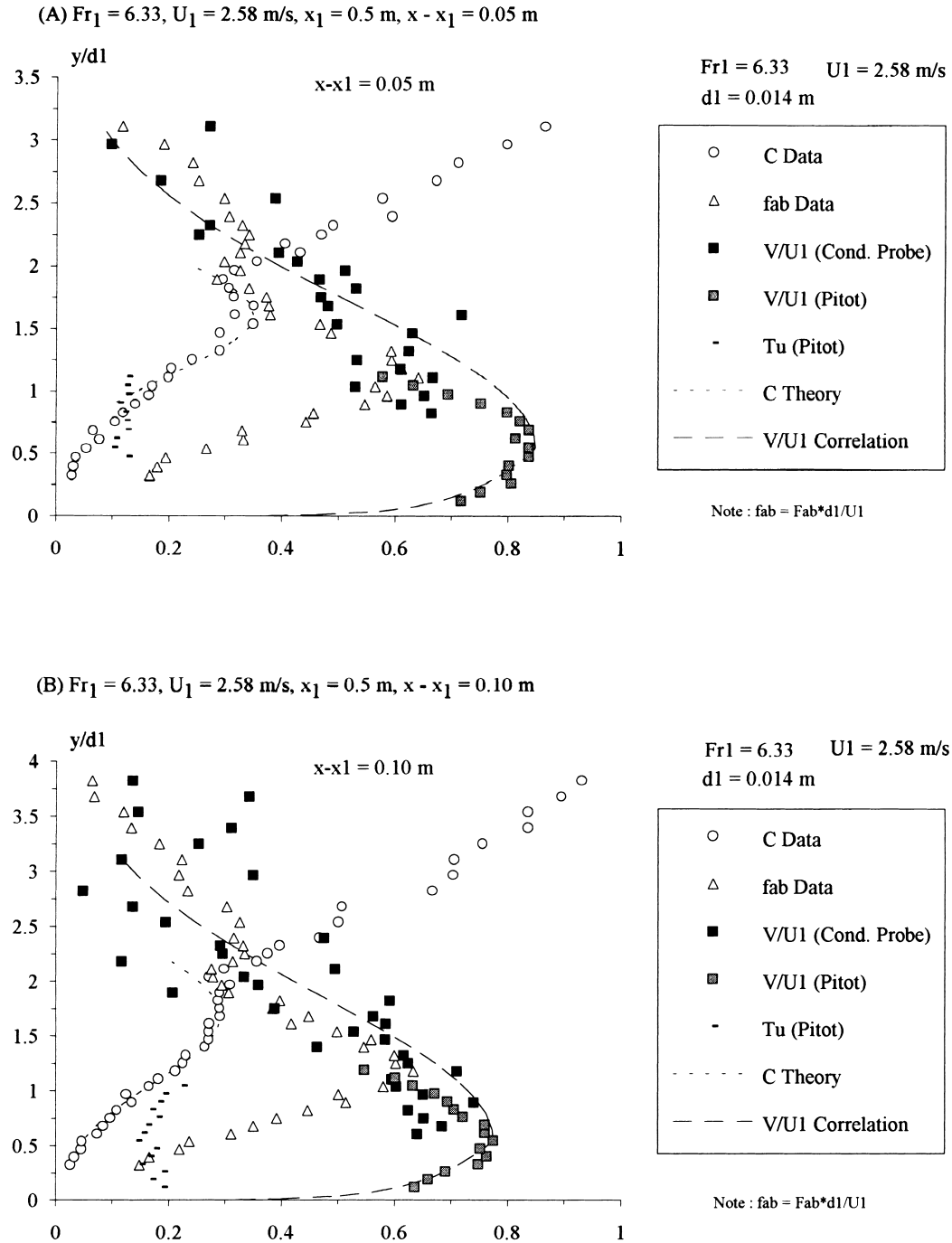
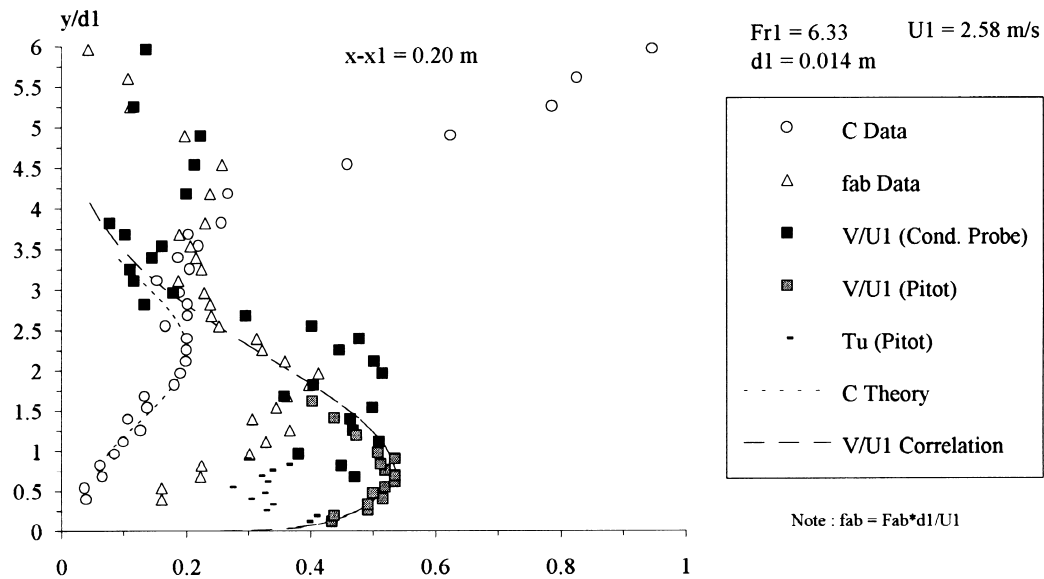


Fig. 2. Typical distributions of air concentration, dimensionless velocity and dimensionless bubble frequency (present study).

(C) $Fr_1 = 6.33$, $U_1 = 2.58$ m/s, $x_1 = 0.5$ m, $x - x_1 = 0.20$ m



(D) $Fr_1 = 8.48$, $U_1 = 3.47$ m/s, $x_1 = 0.5$ m, $x - x_1 = 0.05$ m

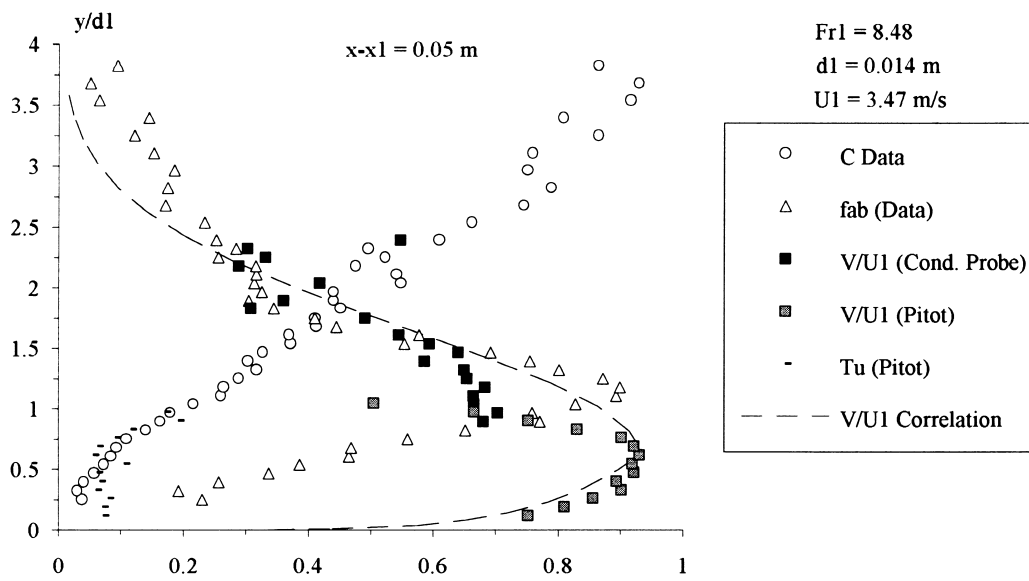
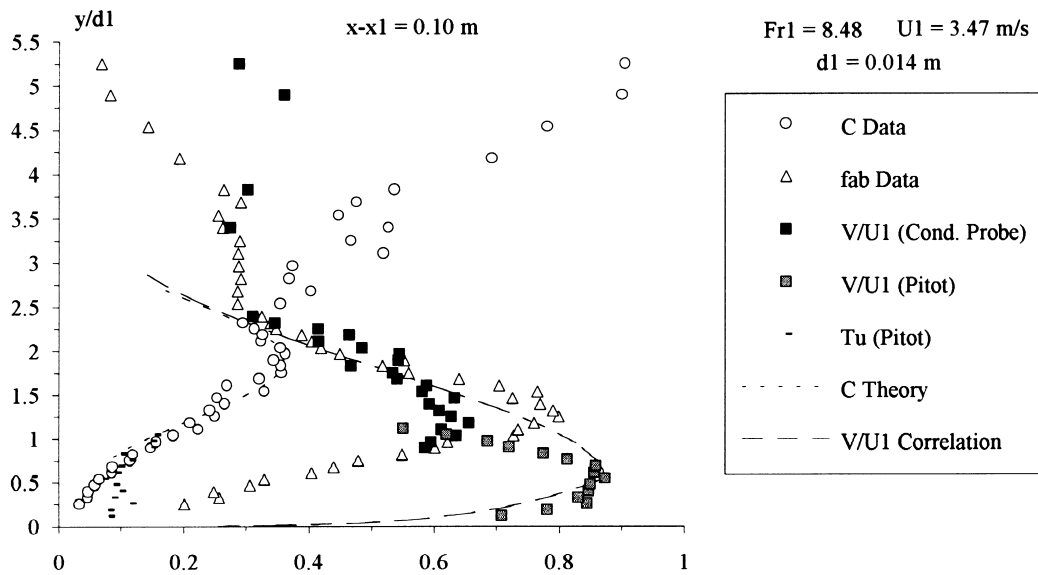


Fig. 2 (continued)

(E) $Fr_1 = 8.48$, $U_1 = 3.47$ m/s, $x_1 = 0.5$ m, $x - x_1 = 0.10$ m



(F) $Fr_1 = 8.48$, $U_1 = 3.47$ m/s, $x_1 = 0.5$ m, $x - x_1 = 0.15$ m

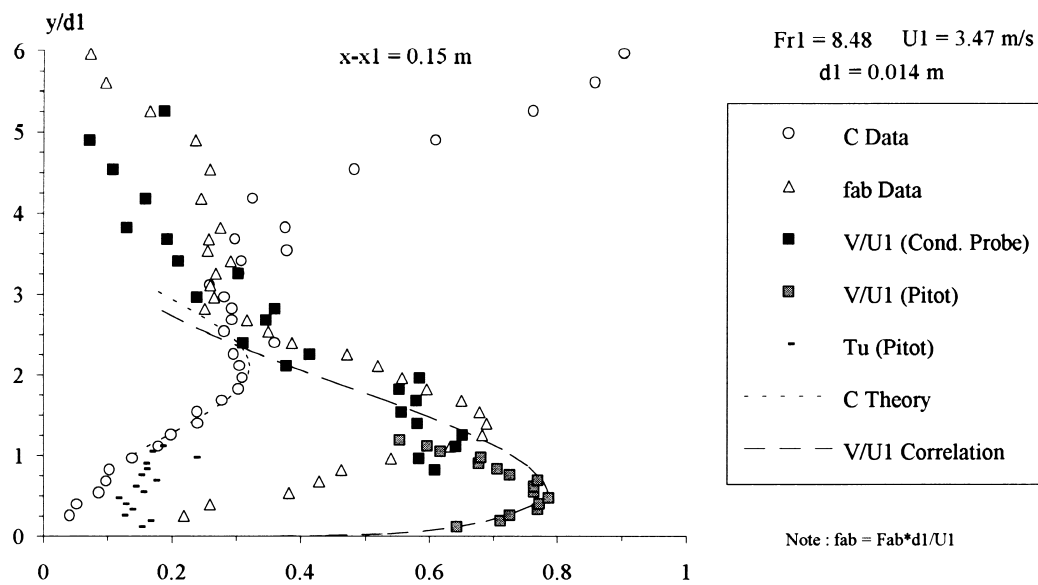


Fig. 2 (continued)

between the impinging flow and the recirculating region. The recirculation region is characterised by strong unsteady recirculation, large bubbles and air packets, and the liquid becomes reduced to a foam structure (i.e., thin films separating the air bubbles) near the free-surface (e.g. Chanson, 1995b, 1997a).

3.2. Void fraction profile in partially-developed jumps

For hydraulic jumps with partially developed inflow conditions, several studies (e.g. Resch and Leutheusser, 1972; Chanson, 1995a,b) showed that the air concentration distributions exhibit a void fraction peak in the turbulent shear region (Figs. 2 and 3). The air concentration data are best correlated by a solution of the diffusion equation (Chanson, 1995a,1997a):

$$C = C_{\max} \times \exp \left[- \frac{1}{4} \frac{U_1 d_1}{D_t} \frac{(y/d_1 - Y_{C_{\max}}/d_1)^2}{(x - x_1)/d_1} \right] \quad \text{for } y/Y_{\text{shear}} < 1 \quad (1)$$

where C_{\max} is the maximum air content in the turbulent shear layer region measured at a distance $Y_{C_{\max}}$ from the bottom, U_1 is the free-stream velocity of the inflow, d_1 is the inflow depth, x and y are the longitudinal and vertical distances measured from the channel intake and bed, respectively, x_1 is the location of the jump toe, D_t is a turbulent diffusivity and Y_{shear} is the upper limit of the turbulent shear region (Fig. 3). Eq. (1) is compared with experimental data in Fig. 2. A good agreement is noted between theory (Eq. (1)) and data, but when approaching $y/Y_{\text{shear}} = 1$. Y_{shear} corresponds to the transition between the shear region and the recirculation region in which air bubble entrainment is not an advective diffusion process.

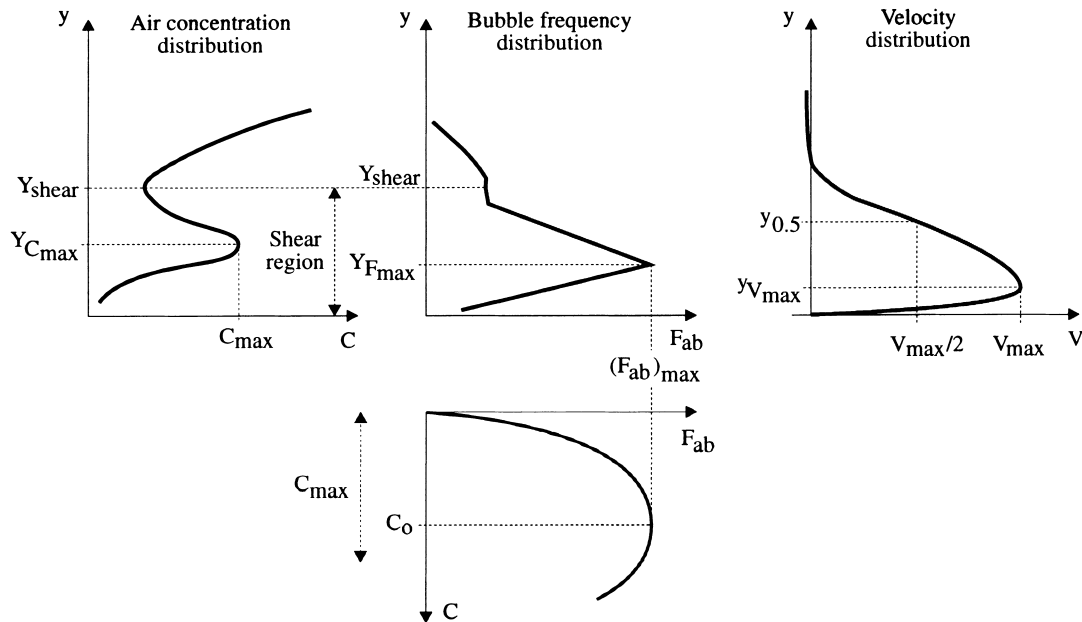


Fig. 3. Definition sketch of the air–water flow properties in hydraulic jump with partially-developed inflow conditions.

For the present study, the upper limit of the turbulent shear region is best correlated by:

$$\frac{Y_{\text{shear}}}{d_1} = 1 + 0.199 \frac{x - x_1}{d_1} \quad \text{for } (x - x_1)/d_1 \leq 28.7 \quad (2)$$

In the shear layer region, the maximum void fraction decreases with distance from the jump toe and the data are correlated by:

$$C_{\text{max}} \propto \left(\frac{x - x_1}{d_1} \right)^m \quad \text{for } (x - x_1)/d_1 \leq 28.7 \quad (3)$$

with $m = -0.58$ and -0.695 for $Fr_1 = 6.3$ and 8.5 , respectively. The position of the maximum air content is independent of the inflow Froude number and it is best correlated by:

$$\frac{Y_{C_{\text{max}}}}{d_1} = 1 + 0.108 \frac{x - x_1}{d_1} \quad \text{for } (x - x_1)/d_1 \leq 28.7 \quad (4)$$

Eq. (4) is shown in Fig. 4 where it is compared with the data (present study) and some re-analysed data. The results indicate a good agreement between all experiments performed with partially-developed inflow conditions. Note that Eq. (4) is close to Chanson's (Chanson, 1995b) correlation validated with both plunging jet and hydraulic jump data (Table 2).

The values of turbulent diffusivity D_t were estimated for each experiment by fitting Eq. (1) to

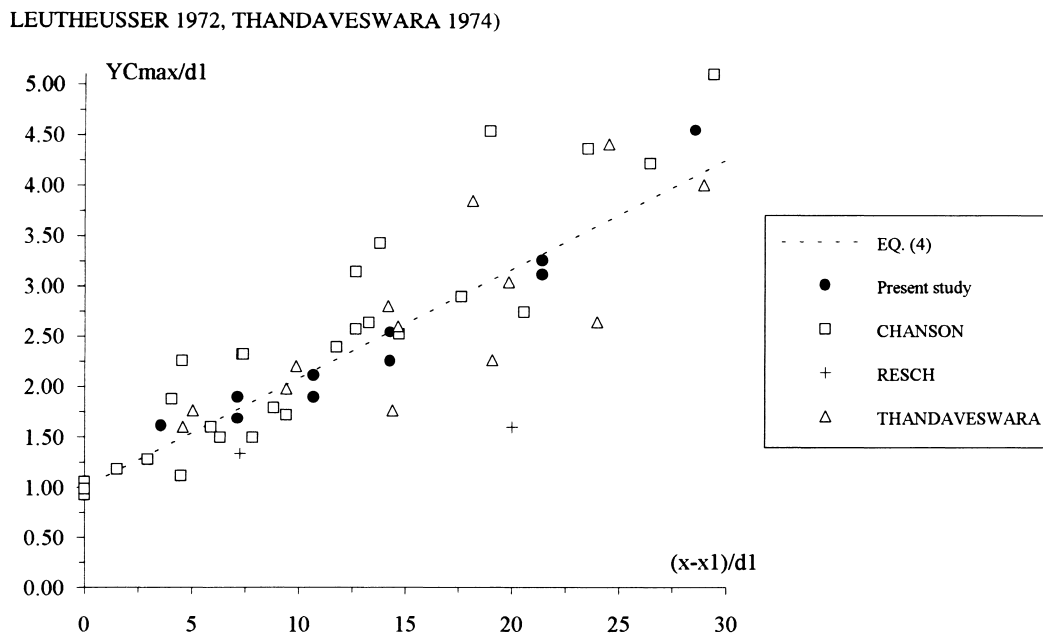


Fig. 4. Location of the maximum air content $Y_{C_{\text{max}}}/d_1$ in hydraulic jump with partially developed inflow conditions: comparison between Eq. (4) and data (present study, Chanson, 1995a; Resch and Leutheusser, 1972, Thandaveswara, 1974).

the data of C (Table 3). Overall they are comparable with a previous investigation performed in the same flume and this suggests a good repeatability of the experiments.

4. Experimental results: air–water velocity profile

4.1. Upstream flow

With partially-developed inflow conditions, the upstream flow consists of a developing bottom boundary layer and an ideal-fluid flow region above (Fig. 1). In the boundary layer,

Table 2
Void fraction distribution in hydraulic jump flows^a

Reference	Correlation	Range	Comments
Chanson (1995b)	$C = C_{\max} \times \exp \left[-2.773 \left(\frac{y - Y_{C_{\max}}}{\Delta Y_{50\%}} \right)^2 \right]$	$\frac{y}{Y_{\text{shear}}} \leq 1$	Validated with author’s plunging jet and hydraulic jump data, page 1117
	$C_{\max} \propto \left(\frac{x - x_1}{d_1} \right)^{-0.54}$	P/D inflow conditions	
	$\frac{Y_{C_{\max}}}{d_1} = 1.1518 + 0.1002 \frac{x - x_1}{d_1}$		Validated with plunging jet and hydraulic jump data, page 1117
	$\frac{\Delta Y_{50\%}}{d_1} = 0.5243 + 0.1689 \frac{x - x_1}{d_1}$		Validated with plunging jet and hydraulic jump data, page 1117
Present study	$C = C_{\max} \times \exp \left[-\frac{1}{4} \frac{V_1 d_1}{D_t} \frac{(y/d_1 - Y_{C_{\max}}/d_1)^2}{(x - x_1)/d_1} \right]$	$\frac{Y}{Y_{\text{shear}}} \leq 1$	Validated with authors’ data
		$\frac{x - x_1}{d_1} \leq 28.7$	
	$C_{\max} \propto \left(\frac{x - x_1}{d_1} \right)^m$	P/D inflow conditions	$m = -0.58$ and -0.695 for $Fr_1 = 6.3$ and 8.5 , respectively
		$\frac{x - x_1}{d_1} \leq 28.7$	
	$\frac{Y_{C_{\max}}}{d_1} = 1 + 0.10815 \frac{x - x_1}{d_1}$	$\frac{x - x_1}{d_1} \leq 28.7$	
	$\frac{Y_{\text{shear}}}{d_1} = 1 + 0.1993 \frac{x - x_1}{d_1}$	$\frac{x - x_1}{d_1} \leq 28.7$	

^a Note: $\Delta Y_{50\%}$: 50%-band width (i.e. where $C = 0.5C_{\max}$).

Table 3

Turbulent diffusivity in the turbulent shear region of hydraulic jumps with partially-developed inflow conditions

Reference	Run	V_1 (m/s)	d_1 (m)	D_t/V_1d_1	$(x - x_1)/d_1$
Chanson (1995a) ^a	C3	1.97	0.0158	1.5E-2	< 7.6
	C2	2.23	0.0158	6.2E-2	< 9.5
	P10	2.47	0.017	6.1E-2	< 23
	C1	3.16	0.0158	5.0E-2	< 12.6
	C0	3.19	0.0158	5.2E-2	< 19
Present study	T6_3	2.34	0.014	3.0E-2	< 14.3
	T8_5	3.14	0.014	4.5E-2	< 21.4

^a Analysis by Chanson (1997a).

the velocity distribution $V(y)$ may be approximated by a power law:

$$\frac{V}{U_1} = \left(\frac{y}{d_1}\right)^{1/N_1} \quad \text{upstream boundary layer} \quad (5)$$

where U_1 is the free-stream velocity and d_1 is the upstream flow depth. For both experiments, the authors observed: $N_1 = 6.45$. This result is close to the findings of Chanson and Qiao (Chanson and Qiao, 1994, Fig. 4-5) in the same flume.

4.2. Velocity distribution in the jump

The authors measured the velocity distributions in the jump using a Pitot tube in the clear water region and a dual-tip conductivity probe in the air–water region. The latter technique gives mean air–water interfacial velocities. Fig. 2 presents typical results. Note the scatter of conductivity probe data which is caused by the ‘boiling’ nature of the jump roller. The double-tip conductivity probe is designed to have the two tips aligned along the streamline. In the recirculation region, the cross-correlation between the probe tips becomes low because of the unsteady and fluctuating nature of the flow, and the data scatter is large.

At each cross-section, the velocity data are best correlated by:

$$\frac{V}{V_{\max}} = \left(\frac{y}{y_{V_{\max}}}\right)^{1/N} \quad \text{for } y/y_{V_{\max}} < 1 \quad (6)$$

$$\frac{V}{V_{\max}} = \exp\left\{-\frac{1}{2}\left[1.765\left(\frac{y - y_{V_{\max}}}{y_{0.5}}\right)\right]^2\right\} \quad \text{for } 1 < y/y_{V_{\max}} < 3 \text{ to } 4 \quad (7)$$

where V_{\max} is the maximum velocity measured at a distance $y_{V_{\max}}$ from the bottom and $y_{0.5}$ is the location where $V = 0.5V_{\max}$ (Fig. 3). For their experiments, the authors obtained $N = 6.43$ or $Fr_1 = 6.3$ and $N = 5.24$ for $Fr_1 = 8.5$. Note that Eq. (7) was first developed by Ohtsu et al. (1990) (Table 4).

For the present study, the characteristic parameters of the velocity profiles are best correlated by:

$$\frac{V_{\max}}{V_1} = 1.08 - 0.027 \frac{x - x_1}{d_1} \quad \text{for } (x - x_1)/d_1 \leq 21.4 \quad (8)$$

$$\frac{y_{0.5}}{V_1} = 1.39 + 0.109 \frac{x - x_1}{d_1} \quad \text{for } (x - x_1)/d_1 \leq 21.4 \quad (9)$$

$$\frac{y_{V_{\max}}}{y_{0.5}} = 0.251 \quad \text{for } (x - x_1)/d_1 \leq 21.4 \quad (10)$$

$$\frac{y_{0.5}}{Y_{90}} = m' \quad \text{for } (x - x_1)/d_1 \leq 21.4 \quad (11)$$

where $V_1 = q_w/d_1$, $m' = 0.570$ and 0.429 for $Fr_1 = 6.3$ and 8.5 , respectively, and Y_{90} is the upper limit of the roller defined as the distance normal to the bed where $C = 90\%$.

4.3. Comparison with previous studies

Rajaratnam (1965) developed a very interesting analogy between the hydraulic jump and the wall jet. He suggested that the transfer of momentum and the velocity profiles in the jump should be similar to plane turbulent wall jet results (Table 5). His experiments confirmed partially the hypothesis. It is, however, unlikely that his velocity measurement device (i.e. Pitot tube) was accurate in air–water flow (Table 1). Since then, several researchers proposed empirical correlations for the velocity profile (Table 4). But most studies used clear-water velocity measurement devices (e.g. Pitot tube, LDV) (Table 1) and little accurate information is available in the air–water flow region.

The present data confirm Rajaratnam's (Rajaratnam, 1965) analogy of velocity profile between hydraulic jump and wall jet. The results suggest, however, that the characteristic parameters of the air–water velocity distribution (i.e. Eqs. (6)–(11)) differ quantitatively from monophasic flow results (Table 5).

The main characteristics of the velocity profiles are summarised in Figs. 5–7. In each figure, the data (present study) are compared with the re-analysis of previous studies (Table 1) and Eqs. (8)–(10). Altogether the maximum velocity decreases linearly with the distance from the jump toe and for $(x - x_1)/d_1 < 30$ (Fig. 5). Fig. 6 presents the dimensionless distance $y_{0.5}/d_1$ where $V = 0.5V_{\max}$. The data (Present study) are consistently larger than past results. Based upon their own experience (e.g. Chanson and Brattberg, 1997,1998), the writers believe that previous studies could not estimate accurately $y_{0.5}$ because of measurements errors: the air content is substantial at the location where $V = 0.5V_{\max}$ and clear-water instrumentation would be inaccurate. Fig. 7 suggests that the ratio $y_{V_{\max}}/y_{0.5}$ is basically independent of the longitudinal distance although the data exhibit some scatter.

Table 4
Empirical correlations of hydraulic jump flow velocity distributions^a

Reference	Correlation	Range	Comments
Rajaratnam (1965)	$\frac{yV_{\max}}{y_{0.5}} = 0.18$	P/D inflow conditions	Validated with author's data (free jump), page 119
Ohtsu et al. (1990)	$\frac{V}{V_{\max}} = \left(\frac{y}{yV_{\max}}\right)^{1/12}$	$\frac{y}{yV_{\max}} < 1$ P/D inflow conditions	Validated with authors' data, page 34
	$\frac{V}{V_{\max}} = \left(\frac{y}{yV_{\max}}\right)^{1/7}$	$\frac{y}{yV_{\max}} < 1$ F/D inflow conditions	Page 34
	$\frac{V}{V_{\max}} = \exp\left\{-\frac{1}{2}\left[1.765\left(\frac{y - yV_{\max}}{y_{0.5}}\right)\right]^2\right\}$	$1 \leq \frac{y}{yV_{\max}} < 4.5$ P/D inflow conditions	Page 34
	$\frac{V}{V_{\max}} = \exp\left\{-\frac{1}{2}\left[1.814\left(\frac{y - yV_{\max}}{y_{0.5}}\right)\right]^2\right\}$	$1 \leq \frac{y}{yV_{\max}} < 4.3$ F/D inflow conditions	Page 34
	$\frac{V_{\max} - V_2}{V_1} = 0.0855 - 1.114 \times \log_{10}\left(\frac{x - x_1}{L_r}\right)$	$0.1 \leq \frac{x - x_1}{L_r} < 4.3$ $2.5 \leq Fr_1 \leq 9.5$	Page 5
	$\frac{yV_{\max}}{y_{0.5}} = 0.333$	P/D and F/D inflow conditions P/D inflow conditions	Page 34
	$\frac{yV_{\max}}{y_{0.5}} = 0.351$	F/D inflow conditions	Page 34
	$\frac{y_{0.5}}{d_1} = \frac{0.330}{\sqrt{Fr_1}} \times \frac{x - x_1}{d_1}$	$3 \leq Fr_1 \leq 9.5$ $0.1 \leq \frac{x - x_1}{L_r} \leq 7$ P/D inflow conditions	Page 35

	$\frac{y_{0.5}}{d_1} = \frac{0.370}{\sqrt{Fr_1}} \times \frac{x - x_1}{d_1}$	$3 \leq Fr_1 \leq 9.5$	Page 35
Hager (1992)	$\frac{V}{V_{\max}} = 2 \left[\frac{5y}{y_{0.5}} \times \exp \left(1 - \frac{5y}{y_{0.5}} \right) \right]^{0.12}$	$0.1 \leq \frac{x - x_1}{L_r} \leq 7$ F/D inflow conditions $8.3 \leq \frac{x - x_1}{d_1} \leq 41.7$	Validated with data from Rajaratnam (1965), page 20
	$\frac{V_{\max}}{V_1} = \frac{1}{42} \left(45 - \frac{x - x_1}{d_1} \right)$	$3.9 \leq Fr_1 \leq 9.05$ $\frac{x - x_1}{d_1} \leq 30$	
	$\frac{y_{0.5}}{d_1} = 1 + \frac{1}{15} \frac{x - x_1}{d_1}$	$\frac{x - x_1}{d_1} \leq 30$	
	$\frac{V - V_{\min}}{V_{\max} - V_{\min}} = \left[\cos \left(100 \times \frac{y - y_{V_{\max}}}{d_2 - y_{V_{\max}}} \right) \right]^2$	$4.3 \leq Fr_1 \leq 8.9$	Validated with author's data, page 21
	$\frac{V_{\max} - V_2}{V_1 - V_1} = \exp \left[-2 \left(\frac{x - x_1}{L_r} \right)^{1.8} \right]$	$0 \leq \frac{x - x_1}{L_r} \leq 1.4$	Page 22
	$\frac{V_{\min}}{V_2} = -\sin \left[\frac{1}{1.1} \left(0.1 + \frac{x - x_1}{L_r} \right) \right]$	$0.05 \leq \frac{x_1}{L_r} \leq 1.4$	Page 22
	$\frac{y_{V_{\max}}}{d_2 - d_1} = 0.06 \left[1 + 5 \left(\frac{x - x_1}{L_r} - \frac{1}{4} \right)^2 \right]$	$0.05 \leq \frac{x - x_1}{L_r} \leq 1.2$	Page 23
Chanson (1995b)	$\frac{y_{0.5}}{d_1} = 1 + 0.0805 \frac{x - x_1}{d_1}$		Re-analysis of data of Rajaratnam (1965)
	$\frac{y_{0.5}}{d_1} = 1 + 0.0737 \frac{x - x_1}{d_1}$	P/D inflow conditions	Re-analysis of data from Ohtsu et al. (1990)

(continued on next page)

Table 4 (continued)

Reference	Correlation	Range	Comments
	$\frac{y_{0.5}}{d_1} = 1 + 0.114 \frac{x - x_1}{d_1}$	F/D inflow conditions	Re-analysis of data from Ohtsu et al. (1990)
Present study	$\frac{V}{V_{\max}} = \left(\frac{y}{y_{V_{\max}}} \right)^{1/N}$	$y/y_{V_{\max}} < 1$ P/D inflow conditions	Validated with the authors' data
	$\frac{V}{V_{\max}} = \exp \left\{ -\frac{1}{2} \left[1.765 \left(\frac{y - y_{V_{\max}}}{y_{0.5}} \right) \right]^2 \right\}$	$1 < y/y_{V_{\max}} < 3$ to 4 $(x - x_1)/d_1 \leq 21.4$ P/D inflow conditions $(x - x_1)/d_1 \leq 21.4$	Correlation developed by Ohtsu et al. (1990)
	$\frac{V_{\max}}{V_1} = 1.083 - 0.0268 \frac{x - x_1}{d_1}$	$(x - x_1)/d_1 \leq 21.4$	
	$\frac{y_{0.5}}{d_1} = 1.391 + 0.1093 \frac{x - x_1}{d_1}$	$(x - x_1)/d_1 \leq 21.4$	
	$\frac{y_{V_{\max}}}{y_{0.5}} = 0.2509$	$(x - x_1)/d_1 \leq 21.4$	
	$\frac{y_{0.5}}{Y_{90}} = m'$	$(x - x_1)/d_1 \leq 21.4$	$m' = 0.5696$ and 0.4291 for $Fr_1 = 6.3$ and 8.5 , respectively

^a d_2 : downstream flow depth; $erf(u) = \frac{2}{\sqrt{\pi}} \int_0^u \exp(-t^2) dt$; L_r : roller length; V_2 : downstream flow velocity; P/D: partially developed inflow conditions; F/D: fully-developed inflow conditions.

Table 5
Empirical correlations of wall jet velocity distributions^a

Reference	Correlation	Range	Comments
Rajaratnam (1976)	$\frac{V}{V_{\max}} = \left(\frac{y}{yV_{\max}}\right)^{1/4}$	$\frac{y}{yV_{\max}} < 1$	Validated with wall jet data (Myers et al., 1961; Schwarz and Cosart, 1961), page 216
	$\frac{V}{V_{\max}} = 1.48 \left(\frac{y}{y_{0.5}}\right)^{1/7} \left[1 - \operatorname{erf}\left(0.68 \frac{y}{y_{0.5}}\right)\right]$	$\frac{y}{yV_{\max}} > 1$	Page 217
	$\frac{V_{\max}}{V_1} = \frac{3.5}{\sqrt{x/d_1}}$	$\frac{x}{d_1} \leq 100$	Page 219
	$\frac{y_{0.5}}{x} = 0.068$		Page 219

^a $\operatorname{erf}(u) = \frac{2}{\sqrt{\pi}} \int_0^u \exp(-t^2) dt$.

5. Experimental results: air bubble frequency distribution

The authors investigated also the distributions of air bubble frequency. The data provide additional information on the structure of the air–water flow.

The experimental results exhibit a characteristic profile (Figs. 2 and 3): i.e., a triangular profile in the turbulent shear region, a brusque change of slope at the upper edge of the shear

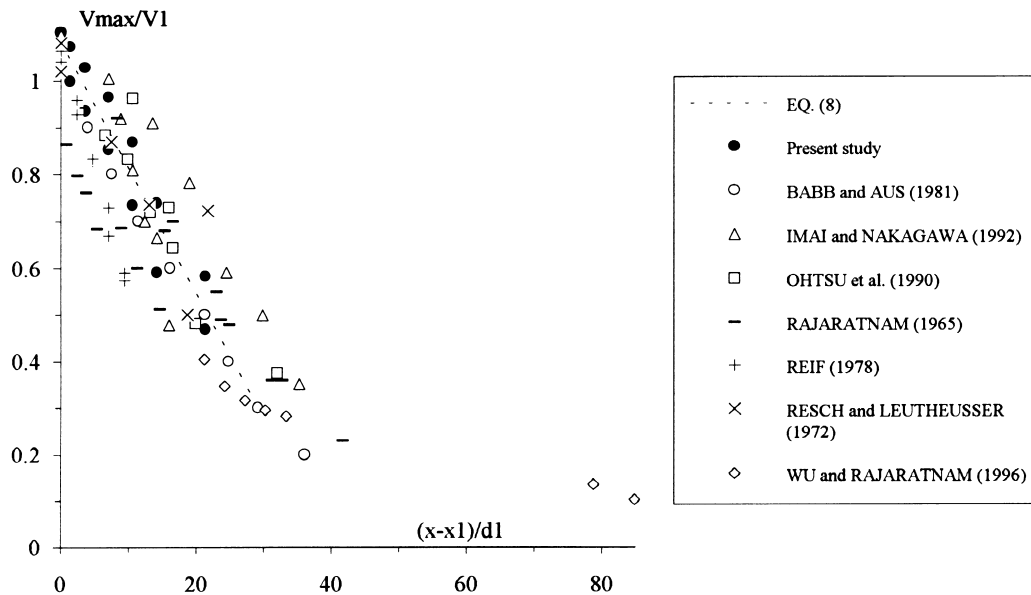


Fig. 5. Dimensionless maximum velocity V_{\max}/V_1 : comparison between data (Table 1) and Eq. (8).

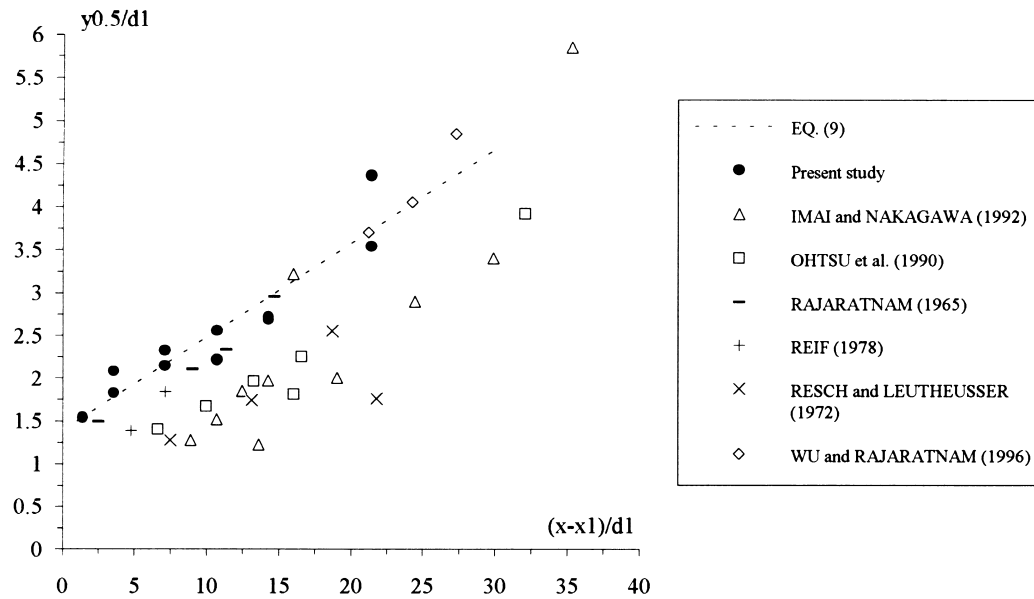


Fig. 6. Dimensionless distance $y_{0.5}/d_1$: comparison between data (Table 1) and Eq. (9).

region and a flatter shape in the recirculation region. The authors believe that the brusque change of shape of the bubble frequency distribution is related to a change of air–water flow structure. Visual observations through the sidewalls and high-speed photographs (e.g. Chanson, 1995b, 1997a, pp. 74–75 and 80–81) showed that the turbulent shear region is characterised by small bubble sizes (millimetric size typically) while the recirculating region includes both small and large size bubbles, and air–water packets, with a foam structure next to the free-surface. There is some similarity with the transition from bubbly flow to plug or slug flow in horizontal circular pipes.

In the turbulent shear region, the bubble frequency distributions follow a simple triangular shape which might be approximated by:

$$\frac{F_{ab}}{(F_{ab})_{\max}} = \frac{y}{Y_{F_{\max}}} \quad \text{for } y/Y_{F_{\max}} < 1 \quad (12a)$$

$$\frac{F_{ab}}{(F_{ab})_{\max}} = 2 - \frac{y}{Y_{F_{\max}}} \quad \text{for } 1 < y/Y_{F_{\max}} < Y_{\text{shear}}/Y_{F_{\max}} \quad (12b)$$

where $(F_{ab})_{\max}$ is the maximum bubble frequency observed at a distance $Y_{F_{\max}}$ from the bottom and Y_{shear} is the upper limit of the turbulent shear region (Eq. (2)). The location of the maximum bubble frequency is best correlated by:

$$\frac{Y_{F_{\max}}}{d_1} = 1 + 0.0346 \left(\frac{x - x_1}{d_1} \right)^{1.17} \quad \text{for } (x - x_1)/d_1 \leq 28.7 \quad (13)$$

The maximum bubble frequency was observed to decay exponentially with the distance from

the jump toe:

$$\frac{(F_{ab})_{\max} \times d_1}{U_1} = 0.117 \times Fr_1 \times \exp\left(-0.0415 \frac{x - x_1}{d_1}\right) \quad \text{for } (x - x_1)/d_1 \leq 28.7 \quad (14)$$

5.1. Remarks

The bubble frequency distribution may be presented also as a function of the air content. The data (Fig. 8) exhibit a characteristic parabolic shape which is best fitted by:

$$\frac{F_{ab}}{(F_{ab})_{\max}} = 1 - \left(1 - \frac{C}{C_o}\right)^2 \quad \text{for } 1.4 \leq (x - x_1)/d_1 \leq 28.7 \quad (15)$$

where C_o is the air content at the maximum bubble frequency (Fig. 3). C_o may be correlated as:

$$\frac{C_o}{C_{\max}} = 0.587 + 0.0135 \frac{x - x_1}{d_1} \quad \text{for } 3.6 \leq (x - x_1)/d_1 \leq 28.7 \quad (16)$$

where C_{\max} is the maximum air content in the turbulent shear layer (Fig. 3, Eq. (3)). Note that such a parabolic shape (i.e. Eq. (15)) was observed also in high-velocity water jets (Brattberg et al., 1998) and in open channel flows (Chanson, 1997b). The result suggests a similarity of air-water flow patterns between the three flow situations.

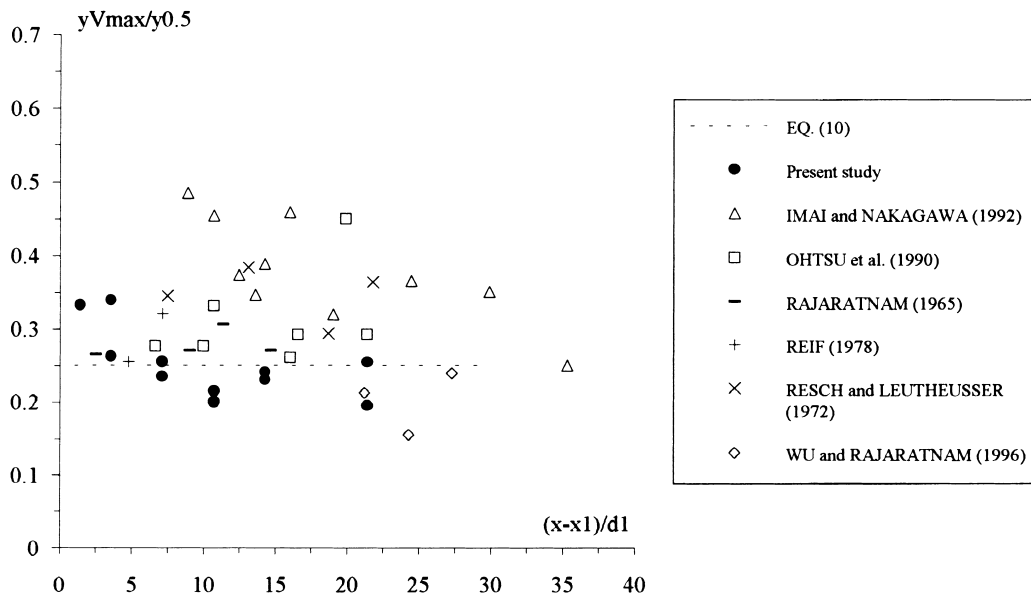
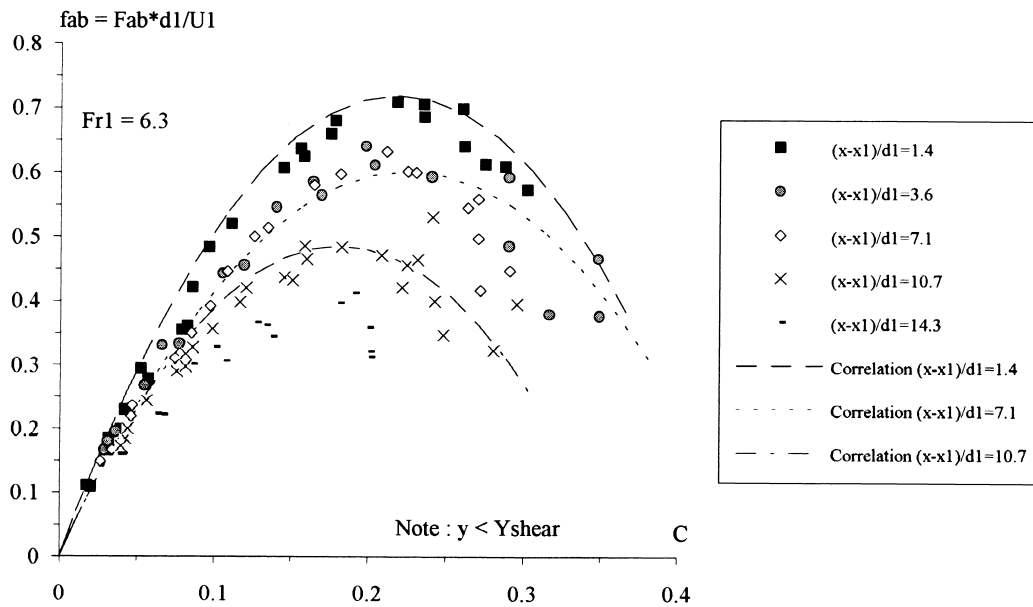


Fig. 7. Dimensionless distance $y_{V_{\max}}/y_{0.5}$: comparison between data (Table 1) and Eq. (10).

(A) $Fr_1 = 6.33$, $U_1 = 2.58$ m/s, $x_1 = 0.5$ m



(B) $Fr_1 = 8.48$, $U_1 = 3.47$ m/s, $x_1 = 0.5$ m

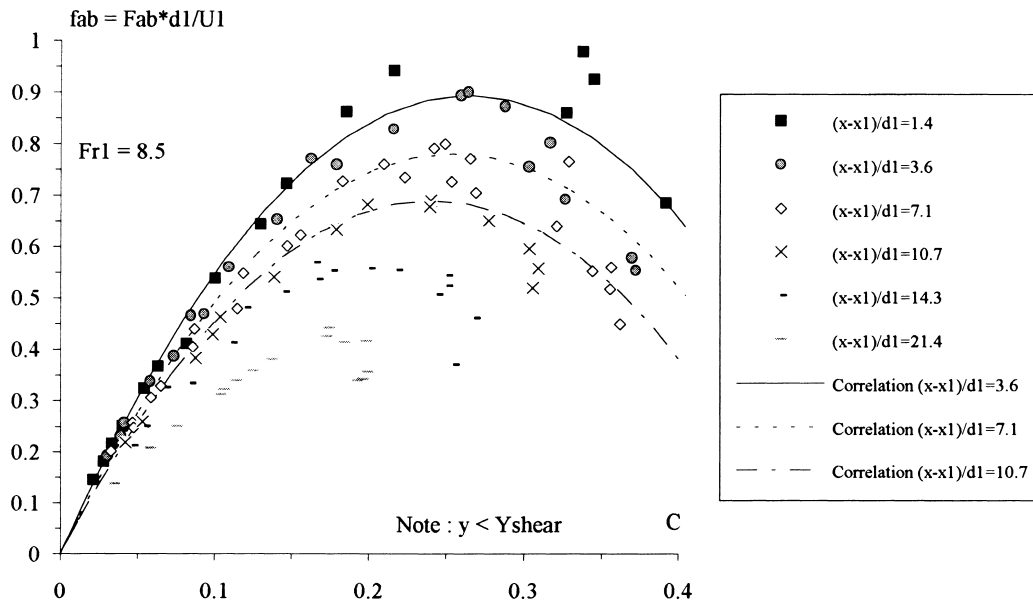


Fig. 8. Dimensionless bubble frequency ($f_{ab} = F_{ab} \times d_1 / U_1$) distribution in the turbulent shear region as a function of the local air content C —comparison with Eq. (15).

6. Discussion

A hydraulic jump is an unsteady dynamic process characterised by longitudinal fluctuations of the jump toe. Mossa and Tolve (1998) presented flow pictures, suggesting that the jump fluctuations are associated with a vortex pairing mechanism. During the experiments, the probes were fixed and did not follow the longitudinal oscillations. The present data (e.g. Fig. 2, 5 and 8) exhibit a greater scatter than the probe accuracy, reflecting the fluctuating nature of the investigated flow.

In the air–water region, the position of the air diffusion layer may be compared with the region of momentum transfer. The locations of the maximum velocity, maximum bubble frequency and maximum air content (in the turbulent shear region) satisfy consistently:

$$\frac{yV_{\max}}{d_1} < \frac{Y_{F_{\max}}}{d_1} < \frac{Y_{C_{\max}}}{d_1} < \frac{y_{0.5}}{d_1} \quad \text{for } (x - x_1)/d_1 \leq 28.7 \quad (17)$$

The relationship is illustrated in Fig. 9 where the data are plotted with the empirical correlations.

Fig. 9 and Eq. (14) imply that most air entrained in the shear layer is advected in the high-velocity region (i.e. $V_{\max}/2 < V_{\max}$). Note the similarity with plunging jet flows (Chanson, 1995a, 1997a) in which experimental observations indicated: $Y_{C_{\max}} < y(V = V_{\max}/2)$. Further Eq. (17) implies that the location of maximum void fraction ($y = Y_{C_{\max}}$) is associated with larger bubble sizes (and/or lower velocities) than the location of maximum bubble count ($y = Y_{F_{\max}}$).

6.1. Local aeration: analogy between hydraulic jumps and plunging jets

Chanson (1995b) developed a complete analogy between vertical plunging jet flows and hydraulic jumps in horizontal channel with partially-developed inflow (Fig. 10). The present study confirms the similarity and it identifies some notable differences.

In the developing shear region, the distributions of air bubble concentration follow the same relationship, both qualitatively and quantitatively (i.e. Eq. (1)). The location of the symmetry line of the air diffusion layer is nearly identical:

$$\frac{Y_{C_{\max}}}{d_1} = 1 + 0.108 \frac{x - x_1}{d_1} \quad \text{hydraulic jump flow } ((x - x_1)/d_1 \leq 28.7)$$

$$\frac{Y_{C_{\max}}}{d_1} = 1.19 + 0.064 \frac{x - x_1}{d_1} \quad \text{plunging jet flow} \quad (18)$$

Values of the turbulent diffusivities D_t are close between the two types of air–water flows. For example, $D_t/(U_1 \times d_1) = 0.04$ and 0.02 for a hydraulic jump flow with $U_1 = 3.47$ m/s and for a plunging jet flow with $U_1 = 3$ m/s, respectively (Chanson and Brattberg, 1997).

In both flow situations, the maximum air concentration in the air diffusion layer decays exponentially with the longitudinal distance:

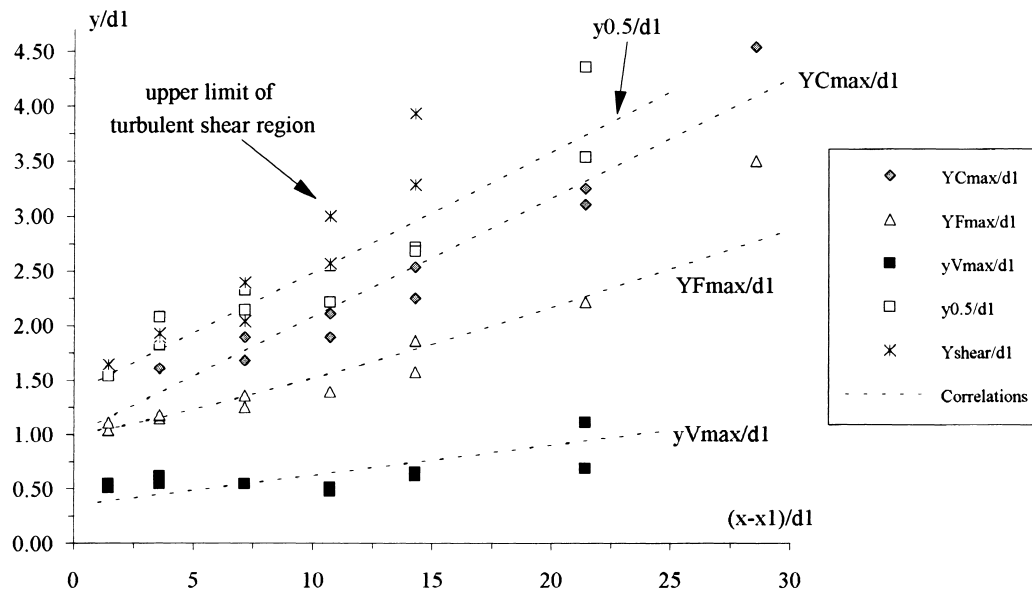


Fig. 9. Dimensionless characteristic parameters as functions of the dimensionless distance from the jump toe— Comparison with empirical correlations (Eqs. (2), (4), (9), (10) and (13)).

$$C_{max} \propto \left(\frac{x - x_1}{d_1} \right)^{-m'} \quad \text{hydraulic jump flow and plunging jet flow}$$

with m' varying from 0.4 to 0.7.

Hydraulic jumps and supported plunging jets are developing shear flows (Fig. 10). The mixing layer centreline (i.e. streamline where $V = 0.5V_{max}$) corresponds approximately to the location of maximum shear stress, and its location is almost identical for both types of local aeration:

$$\frac{y_{0.5}}{d_1} = 1.39 + 0.11 \frac{x - x_1}{d_1} \quad \text{hydraulic jump flow } ((x - x_1)/d_1 \leq 21.4)$$

$$\frac{y_{50}}{d_1} = 1.50 + 0.094 \frac{x - x_1}{d_1} \quad \text{plunging jet flow} \tag{19}$$

The transfer of momentum between the jet core and the fluid at rest at infinity is affected by the flow geometry and some differences are expected between a horizontal hydraulic jump and a vertical plunging jet (Fig. 10). In a plunging jet flow, the fluid entrainment into the shear layer causes a 90-degree change in momentum direction of surrounding fluid. In a hydraulic jump, the entrainment of the recirculating fluid into the shear flow induces a 180-degree change in momentum direction of the roller flow. It was thought that the different mode of fluid entrainment into the shear flow could have affected the air diffusion process. This is not the case and the finding suggests that the air entrainment process is predominantly an advective dispersion.

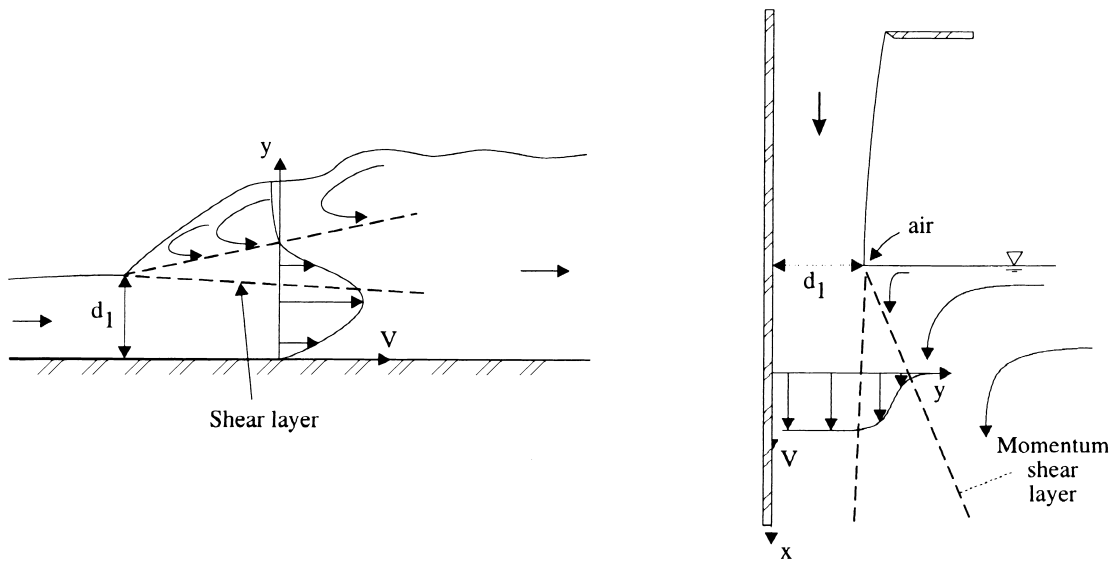


Fig. 10. Transfer of momentum and fluid entrainment process in developing shear layers at hydraulic jump and vertical plunging jet.

Note that, at a given cross-section, the relationship between bubble frequency and air concentration differs between hydraulic jump flow and plunging jet flow. In a plunging jet flow, the bubble frequency and air concentration are not related by an unique parabolic shape (Fig. 8).

7. Conclusion

The authors have described a new study of the air–water flow properties in a hydraulic jump flow. The study is focused on the developing shear layer of hydraulic jumps with partially-developed inflow conditions and new correlations were developed for $x/d_1 \leq 20\text{--}25$.

The present investigation highlights that, with partially-developed inflow conditions, a hydraulic jump is characterised by two air–water flow region with significantly different properties. In the air–water turbulent shear region, the void fraction distribution follows a solution of the diffusion equation and the bubble frequency profile exhibits a triangular shape with a maximum value. In the recirculating region, the air content increases toward 100% (at the free-surface) and the bubble frequency profile follow a different trend which is related to a different air–water flow structure and bubble size composition. An interesting result is the relationship between the air content and the bubble frequency in the turbulent shear region. The present results suggest a parabolic relationship in the shear region as in self-aerated open channel flows and high-velocity water jets discharging into air.

The velocity distribution has a similar shape as wall jet flows (Rajaratnam, 1965) but the quantitative parameters differ. It is believed that they are affected significantly by the air entrainment process.

The results confirms the air–water shear layer analogy between horizontal hydraulic jumps and vertical plunging jets. They suggest that the air–water diffusion process and the momentum transfer in the developing shear flow are little affected by gravity in first approximation.

In the authors' opinion, the study emphasises the complexity of the air–water region of hydraulic jump. Further experimental investigations are required to gain a better understanding of the complete flow field, including with fully-developed inflow conditions.

Acknowledgements

The authors wants to thank particularly Professor C.J. Apelt, University of Queensland, who supported this project since its beginning. They thank also Dr. T. Nakagawa, Kanazawa Institute of Technology (Japan) for providing information of interest. The authors acknowledge the support of the Department of Civil Engineering at the University of Queensland which provided the experimental facilities and the financial support of Australian Research Council (Ref. No. A89331591). The second author was supported by an APA scholarship sponsored by the Australian Research Council (Ref. No. A8941296). The authors thank the reviewers for their helpful comments.

References

- Babb, A.F., Aus, H.C., 1981. Measurements of air in flowing water. *J. Hyd. Div., ASCE* 107 (HY12), 1615–1630.
- Brattberg, T., Toombes, L., Chanson, H., 1998. Developing air–water shear layers of two-dimensional water jets discharging into air. In: *Proc. 1998 ASME Fluids Eng. Conf., FEDSM'98*, Washington DC, USA, June 21–25, Paper FEDSM98-4805, 7.
- Chanson, H., 1995a. Air bubble entrainment in free-surface turbulent flows. Experimental investigations. Report CH46/95, Department of Civil Engineering, University of Queensland, Australia, June, 368.
- Chanson, H., 1995b. Air entrainment in two-dimensional turbulent shear flows with partially developed inflow conditions. *Int. J. of Multiphase Flow* 21 (6), 1107–1121.
- Chanson, H., 1997a. *Air Bubble Entrainment in Free-surface Turbulent Shear Flows*. Academic Press, London, UK, p. 401.
- Chanson, H., 1997b. Air bubble entrainment in open channels. Flow structure and bubble size distributions. *Int. J. of Multiphase Flow* 23 (1), 193–203.
- Chanson, H., Brattberg, T., 1997. Experimental investigations of air bubble entrainment in developing shear layers. Report CH48/97, Department of Civil Engineering, University of Queensland, Australia, July.
- Chanson, H., Brattberg, T., 1998. Air entrainment by two-dimensional plunging jets: the impingement region and the very-near flow field. In: *Proc. 1998 ASME Fluids Eng. Conf., FEDSM'98*, Washington DC, USA, June 21–25. Paper FEDSM98-4806. p. 8.
- Chanson, H., Qiao, G.L., 1994. Air bubble entrainment and gas transfer at hydraulic jumps. Research Report No. CE149, Department of Civil Engineering, University of Queensland, Australia, August, 68.
- Hager, W.H., 1992. *Energy Dissipators and Hydraulic Jump*, 8. Kluwer Academic Publishers, Water Science and Technology Library, Dordrecht, The Netherlands, p. 288.
- Imai, S., Nakagawa, T., 1992. On transverse variation of velocity and bed shear stress in hydraulic jumps in a rectangular open channel. *Acta Mechanica* 93, 191–203.
- Mossa, M., Tolve, U., 1998. Flow visualization in bubbly two-phase hydraulic jump. *J. Fluids Eng., ASME* 120, 160–165.

- Myers, G.E., Schauer, J.J., Eutis, R.H., 1961. The plane turbulent jet. I. Development of friction factor. Technical report, No. 1, Department of Mechanical Engineering, Stanford University, USA.
- Nakagawa, T., 1996. Private Communication, 21 October, 14.
- Ohtsu, I.O., Yasuda, Y., Awazu, S., 1990. Free and submerged hydraulic jumps in rectangular channels. Report of Research Inst. of Science and Technology, No. 35, Nihon University, Japan, February, 50.
- Rajaratnam, N., 1990. The hydraulic jump as a wall jet. *J. of Hyd. Div., ASCE* 91 (HY5), 107–132 Discussion: Vol. 92, No. HY3, pp. 110–123 and Vol. 93, No. HY1, pp. 74–76.
- Rajaratnam, N., 1976. Turbulent jets. In: *Development in Water Science*, 5. Elsevier, New York, USA.
- Reif, T.H., 1978. The effects of drag reducing polymers on the turbulence characteristics of the hydraulic jump. Report EW-11-78, US Naval Academy, Annapolis, USA, 50.
- Resch, F.J., Leutheusser, H.J., 1972. Le ressaut hydraulique: mesure de turbulence dans la region diphasique. (The hydraulic jump: turbulence measurements in the two-phase flow region.) *J. La Houille Blanche*, (4), 279–293 (in French).
- Schwarz, W.H., Cosart, W.P., 1961. The two-dimensional wall-jet. *J. Fluid Mech.* 10 (4), 481–495.
- Thandaveswara, B.S., 1974. Self aerated flow characteristics in developing zones and in hydraulic jumps. Ph.D. thesis, Department of Civil Engineering, Indian Institute of Science, Bangalore, India, 399.
- Wood, I.R., 1990. Air entrainment in free-surface flows. In: *IAHR Hydraulic Structures Design Manual No. 4, Hydraulic Design Considerations*. Balkema, Rotterdam, The Netherlands, p. 149.
- Wu, S., Rajaratnam, N., 1996. Transition from hydraulic jump to open channel flow. *J. of Hyd. Engrg., ASCE* 122 (9), 526–528.